Low-Frequency Calibration of Accelerometers by Rotation in the Gravitational Field at NIST

Jared H. Strait,[1, a)] Richard A. Allen,[1] and Michael Gaitan[1]

Physical Measurement Laboratory, National Institute of Standards and Technology, Gaithersburg, MD 20899

(Dated: 8 March 2026)

We present a low-frequency accelerometer calibration system based on rotation in the gravitational field. Example characterizations of three accelerometers from (0.01 to 1.5) Hz with an uncertainty analysis demonstrate $k = 2$ magnitude and phase uncertainty of <0.1 % and $<0.2°$, respectively. This rotational system complements the linear shakers in the NIST Primary Vibration Calibration Laboratory by improving uncertainty in the range of overlap and extending accelerometer calibration capability to lower frequencies. We demonstrate a magnitude comparison between the linear and rotational approaches, showing agreement to within the rotational calibration uncertainty of <0.1 %.

[a)]Electronic mail: jared.strait@nist.gov

I. INTRODUCTION

In 1954, researchers at the National Bureau of Standards (NBS), the precursor to the National Institute of Standards and Technology (NIST) in the USA, published a paper detailing an accelerometer calibration via rotation in gravity[1]. As they state, "The earth's gravitational field furnishes a convenient sinusoidal forcing function for a vibrating system (e.g. an accelerometer) rotating in a vertical plane." By 1962, however, NBS researchers proclaimed of a linear shaker alternative[2], "The electrodynamic shaker is undoubtedly the most useful calibrator for laboratory use." Although the linear shaker technique improved[3], accelerometer calibration by rotation in gravity (using an instrument called the "earth's field dynamic calibrator," EFDC) continued at NBS through at least 1970 as a complement to linear excitation[4]. At the time, the EFDC required detailed centering and balancing operations for each accelerometer, but it outperformed shakers in certain ways, achieving 0.3 % uncertainty over a portion of the full (0.5 to 45) Hz range[4]. Yet five decades later, electromagnetic shakers coupled with laser interferometers now dominate primary accelerometer calibration laboratories[5,6], valued for their accuracy, ease of use, and frequency range.

Shaker-based measurements, however, are not solely capable of meeting the challenges existing in vibration calibration, for example as outlined in the strategic plan of the Consultative Committee for Acoustics, Ultrasound, and Vibration (CCAUV)[7], including ensuring accuracy and traceability of vibration sensors at low frequency. Uncertainty of shaker-based calibration suffers at the lowest frequencies due to small signal magnitude, where the achievable acceleration magnitude is limited by the shaker stroke length and is thus proportional to the square of the angular frequency, ω^2. This proportionality leaves low-frequency shaker measurements susceptible to low signal-to-noise ratio and the gravity effect, a well-known systematic error[8–10].

In contrast, a rotation-based measurement in gravity achieves a peak stimulus of approximately 9.8 m/s^2 irrespective of frequency. This fact alone establishes an opportunity for a rotation instrument to complement linear shakers in the accelerometer calibration laboratory and to extend the primary calibration range to lower frequencies. Moreover, modern rotational table instruments use closed-loop angular position and velocity feedback to maintain high accuracy even at AC frequencies well below 50 mHz, and they do not require rebalancing between measurements. We have recently used such an instrument for DC

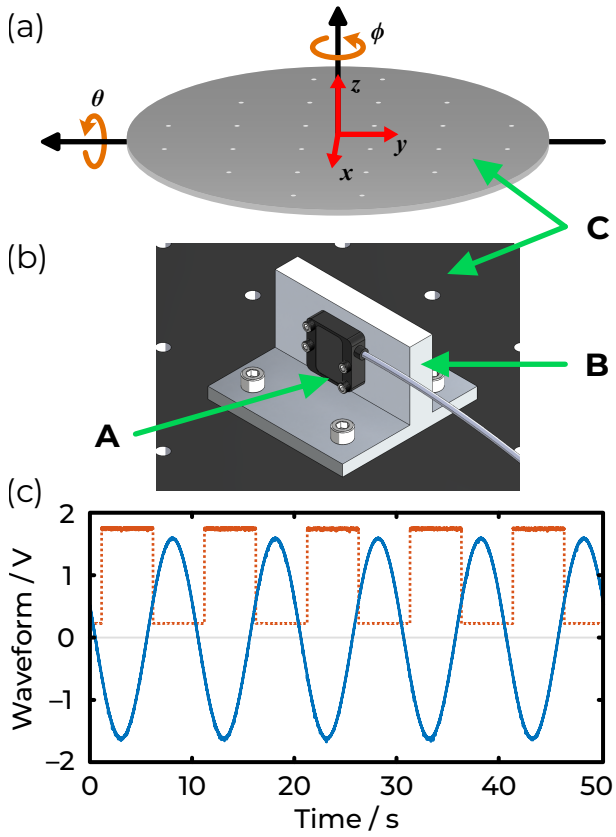

FIG. 1. (a) Diagram of the rotation table (not to scale). The z axis, the table normal, is the ϕ rotation axis; x and y axes lie in the plane of the table. The x, y, and z axes transform under rotations of ϕ and θ. For $\theta = 0$, the z axis is antiparallel to gravity. For $\theta = \pi/2$ and $\phi = 0$, the x axis is parallel to gravity. (b) Visualization of an accelerometer (A) mounted on the 90° bracket (B), bolted to the rotation table (C). Table bolt spacing is 50.8 mm. (c) Example waveforms collected during a 0.1 Hz measurement, including from the accelerometer (solid blue) and the event trigger (red dots).

characterization of 3-axis accelerometers[11–13] as well as an initial study of low-frequency AC measurements[14]. Others have also recently used earth's gravity as a stimulus in calibrations, although generally in different contexts[15–17]. In this article, we describe an accelerometer calibration system (magnitude and phase) based on rotation in gravity using a 2-axis rate table at NIST. This system, a modern version of the EFDC, currently operates from (0 to 1.5) Hz. We provide an uncertainty analysis, and with magnitude uncertainties below 0.1 %, this system outperforms our long-stroke shakers over the operating range.

The method of accelerometer calibration by constant rotation in Earth's gravitational

field determines the magnitude of sensitivity, S given in $\mathrm{V}/(\mathrm{m\,s^{-2}})$, and the signal phase delay with respect to the stimulus, $\Delta\phi$ given in rad or degree, defined here with respect to the mounting surface of the accelerometer package.

$$Se^{i\Delta\phi} = \frac{V_c}{a} \tag{1}$$

where V_c and a, represented as complex phasors, are respectively the corrected accelerometer output voltage and the stimulus acceleration.

Two angles primarily determine the orientation of the nominal sensitive axis (i.e. the axis normal to the accelerometer mounting surface) with respect to gravity (see Fig. 1) and thereby determine the magnitude and phase of the stimulus acceleration:

$$a = g_l \cos(\theta - \pi/2)e^{i\phi} = g_l \sin(\theta)e^{i\phi} \tag{2}$$

where g_l is the local gravitational acceleration, θ is the tilt angle of the normal of the rotation table with respect to g_l, and ϕ is the angle of rotation about the table central axis. The accelerometer is mounted with a 90° bracket such that the nominal sensitive axis is in the x direction, perpendicular to the table normal. The table normal, the z axis, is vertical for $\theta = 0$. Thus, $g_l \sin(\theta)$ and ϕ are respectively the magnitude and phase of stimulus. During operation with constant rotation rate, $\phi = \omega t + \phi_a$ is a linear function of time, where ϕ_a is the stimulus phase at the data collection initiation time, $t = 0$.

Measurements and uncertainty analysis in this article are restricted to the case for which the table rotation axis is set to $\theta = \pi/2$. In Appendix A, we discuss angles $\theta < \pi/2$ and consider the effect of misalignment.

II. METHODOLOGY

A. Apparatus and Data Collection

The new EFDC measurement apparatus centers on a 2-axis commercial rate table (Acutronic AC216-CR[18]) which we use for static positioning of the platform about angle θ and constant rotation about angle ϕ at frequencies from DC to 1.5 Hz. As described above, a 90° mount interfaces the accelerometer under test with the platform; a scale diagram of an example mount and accelerometer appears in Fig. 1(b). Because the sensitive axis of an accelerometer is typically oriented normal to the mounting plane, this mount

positions the sensitive axis in alignment with gravity for $\theta = \pi/2$, as implied by Eq. 2. Appendix A includes an analysis to consider misalignment of the mount.

We define $\arg(a) = \phi = 0$ when the nominal sensitive axis is parallel to gravity (and thus the accelerometer mounting surface is horizontal) with $\theta = \pi/2$. To achieve this in practice, we set both the rate and position encoders of the rate table θ axis to zero and align the accelerometer mount horizontally with a bubble level. A machinist level provides $\approx 0.02°$ accuracy in ϕ.

The rate table instrument provides slip-ring feedthroughs for accelerometer signals and power. In addition, there are two diagnostic outputs: (a) a digital event trigger used as a phase reference (see Sect. II C), which triggers at the known angle $\phi_{\Delta E}$ measured by the rate table position encoder and (b) a waveform used in the uncertainty analysis (see Appendix B 2 e) which is proportional to the ϕ angular velocity error.

We use three voltmeters (Keysight 3458A) to collect the accelerometer, event trigger, and velocity error signals. These voltmeters are configured for DC measurements using a $\leq$100 μs aperture time and external sample triggering driven by the frequency of a separate function generator. This function generator synchronizes data collection between the voltmeters and determines the sampling rate, which varies with rotation frequency to maintain a constant 2000 samples per rotation.

Oversampling the waveforms is beneficial for phase measurement because the event trigger is digital and abruptly transitions from low to high at an unknown time between two samples. The sampling rate thus constrains the event trigger phase measurement, and higher sampling rates correlate with lower Type A phase uncertainty.

A computer controls and queries the rate table, function generator, and voltmeters. Automation software is programmed to loop through an array of frequencies, set the rotation and sampling rates, and retrieve the resulting voltmeter waveforms. We collect 5 sinusoidal cycles per waveform and 10 waveforms at each frequency for statistics. Typical accelerometer signal and event trigger waveforms appear in Fig. 1(c). We commonly use a quasi-logarithmic frequency array ranging from (0.01 to 1.5) Hz. At each frequency, we repeat the measurement for clockwise and counterclockwise rotation directions.

For the following demonstration measurements, we tested three micro-electromechanical systems (MEMS)-based, DC-sensitive, accelerometers labeled I, II, and III. Accelerometer I has a nominal sensitivity of 0.08 V/(m s^{-2}), and accelerometers II and III are two channels

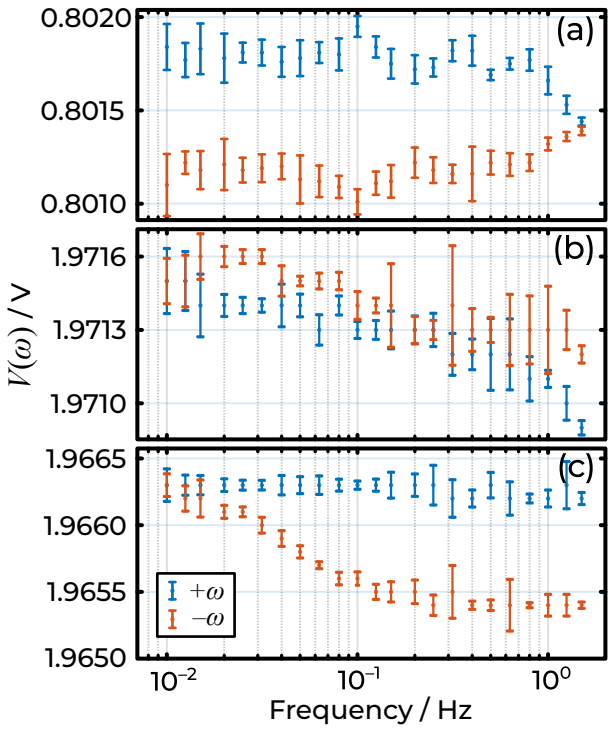

FIG. 2. Extracted signal magnitudes versus frequency for clockwise ($+\omega$) and counterclockwise ($-\omega$) motion of the three accelerometers under test. Error bars are the standard deviation among measurements at each frequency. Differences between $+\omega$ and $-\omega$ signals, typically <1 mV, are inconsistent between accelerometers (a) I, (b) II, and (c) III.

of a three-axis accelerometer with nominal sensitivity 0.2 V/(m s^{-2}).

B. Magnitude Analysis

We are interested in extracting the magnitude sensitivity $S(\omega)$, notated here as a function of the angular frequency of rotation, ω (and using $\theta = \pi/2$):

$$S(\omega) = |V_c(\omega)|/g_l. \tag{3}$$

The initial outcome of the constant rotation measurement is a set of sinusoidal voltage waveforms $V_m(t)$. We then extract waveform magnitudes by calculating the Fourier transform of $V_m(t)$ and selecting the complex magnitude at the revolution frequency ω (this is equivalent to sine-wave fitting[19]). To calculate $S(\omega)$, we correct $V_m(\omega)$ to find $V_c(\omega)$ as described in the following.

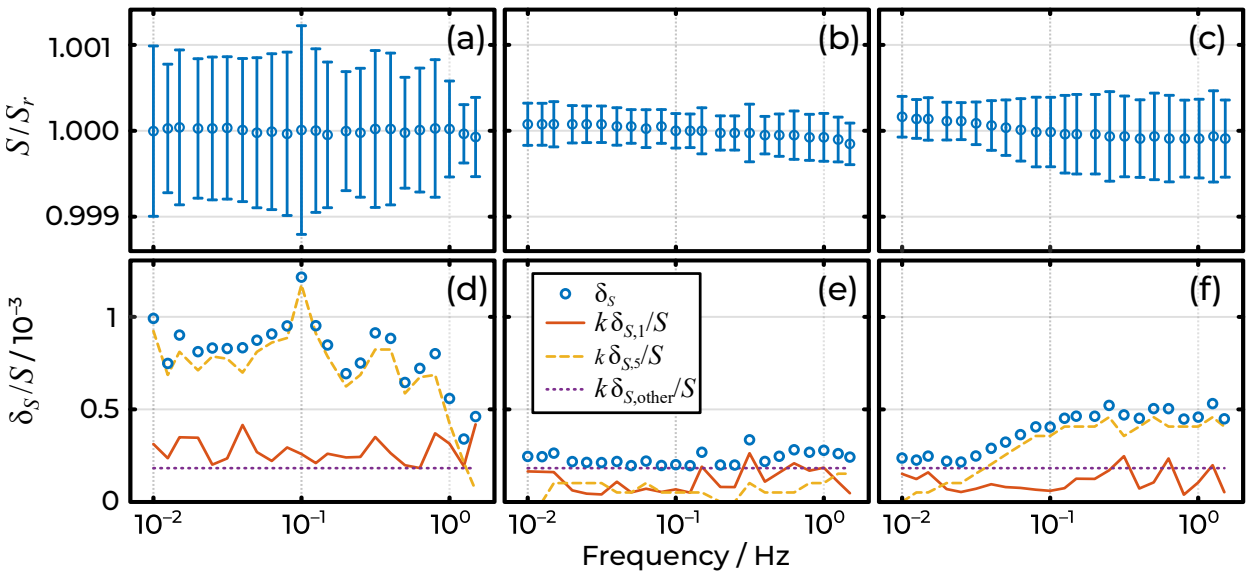

FIG. 3. (a-c) Normalized accelerometer sensitivities versus frequency with $k = 2$ expanded error bars. (a) Accelerometer I, $S_r = 81.774$ mV/(m s^{-2}). (b) Accelerometer II, $S_r = 201.14$ mV/(m s^{-2}). (c) Accelerometer III, $S_r = 200.59$ mV/(m s^{-2}). (d-f) Corresponding $k = 2$ relative uncertainty versus frequency. Included are the total uncertainty (blue circles) and constituent uncertainty components from Type A (solid red), odd-symmetric signal (yellow dashes), and all others (purple dots).

Figure 2 shows example mean magnitudes of $V_m(\omega)$ with standard deviation error bars for the three accelerometers under test. As seen in the figure, we have observed systematic differences between accelerometer voltage magnitudes measured using clockwise and counterclockwise rotation directions, here referenced by positive and negative frequencies respectively. That is, $|V_m(\omega)| \neq |V_m(-\omega)|$, with a difference generally of the order 1 mV or less, compared to mean signals $\approx$(0.8 and 2) V for the tested devices.

We decompose the voltage signals into components with even (+) and odd (−) symmetry with respect to frequency:

$$|V_m(\omega)| = |V_+(\omega)| + |V_-(\omega)|, \tag{4}$$

where

$$\begin{aligned} |V_+(\omega)| &= (|V_m(\omega)| + |V_m(-\omega)|)/2 \\ |V_-(\omega)| &= (|V_m(\omega)| - |V_m(-\omega)|)/2. \end{aligned} \tag{5}$$

We have found that $|V_-(\omega)|$ is accelerometer- and frequency-dependent, and so far $|V_-(\omega)|/|V_+(\omega)| < 0.05$ % in all cases. Since an ideal accelerometer will have $|V_-(\omega)| = 0$,

for Eq. 1 we set

$$|V_c(\omega)| = |V_+(\omega)|. \tag{6}$$

If we have reason to believe that an accelerometer under test has no chiral sensitivity on the order of 0.01 % of the mean sensitivity, then we regard $|V_-(\omega)|$ as indicative of an extrinsic systematic error (such as sensitivity to magnetic field from the rotation motor). In this case, the computation of $|V_+(\omega)|$ effectively cancels this error and $|V_-(\omega)|$ does not add uncertainty. Alternatively, if we wish to make no assumptions about the accelerometer, then we do include $|V_-(\omega)|$ as a term in the magnitude uncertainty (see Section III A).

Figures 3(a-c) display the normalized mean sensitivities $S(\omega)/S_r$, where the reference sensitivity for each accelerometer, S_r, is the mean of $S(\omega)$ across frequency. The error bars are the $k = 2$ expanded uncertainties of the mean, divided by S_r. The values of S_r listed in the Fig. 3 caption have been calculated using Eq. 3 with $g_l = 9.80101$ m/s^2 (see Appendix B 4). Figures 3(d-f) indicate the $k = 2$ uncertainties and some of the subcomponents contributing to the total uncertainty. These uncertainties are the subject of Section III A and Appendix B.

C. Phase Analysis

The calibration extracts the frequency-dependent phase delay between the accelerometer signal and the stimulus:

$$\Delta\phi = \phi_V - \phi_a \tag{7}$$

where ϕ_V and ϕ_a are the constant phase offsets of the accelerometer signal and accelerometer stimulus, respectively. Phase ϕ_V derives from the measured accelerometer voltage phase ϕ_{Vm}, and ϕ_a derives from the event trigger signal phase ϕ_E. Analogously to the magnitude analysis (Section II B), we extract ϕ_{Vm} and ϕ_E as the phase of the complex magnitudes at the revolution frequency, following Fourier transform of the accelerometer and event trigger voltage waveforms. We then correct ϕ_{Vm} and ϕ_E to derive ϕ_V and ϕ_a as described in the following.

A subtlety in the calculation of Eq. 7 arises with a misalignment of the accelerometer axis of sensitivity with respect to the mounting surface normal. Since the calibration phase is defined with respect to the case, misalignment by an angle ϕ_I in the plane of rotation (the x-y plane) will cause a systematic error phase shift of ϕ_I in this rotational-frame measurement

which must be corrected:

$$\phi_V = \phi_{Vm} - \phi_I. \tag{8}$$

For a sense of the size of this correction, in the case that the cross-axis accelerometer sensitivity is driven by misalignment of the sensitivity axis, then the relative cross-axis sensitivity in the x-y plane equals ϕ_I in the small angle approximation. For an upper-limit cross-axis sensitivity of 3 %, $\phi_I \approx 0.03$ rad $\approx 1.7°$.

We empirically determine ϕ_I for each accelerometer by performing a series of DC accelerometer voltage measurements, incrementing ϕ in $\pi/36$ rad steps, with a 5 second pause between steps, over the range $\phi = (0 \text{ to } 2\pi)$ rad. We perform a sine fit over the resulting signal amplitudes versus encoder position. Since the earlier leveling procedure establishes the alignment of the case with gravity at encoder position zero, the phase of the sine fit is ϕ_I. In many cases ϕ_I is much smaller than 1.7°.

Similarly, we measure the phase of the event trigger (ϕ_E) to represent the stimulus; but we must correct for the difference in angle, $\phi_{\Delta E}$, between the event trigger and the defined zero phase. As described in Section II A, alignment of the accelerometer mount with a bubble level at the zero position of the rotational encoder sets the absolute phase reference. So,

$$\phi_a = \phi_E - \phi_{\Delta E}. \tag{9}$$

Finally,

$$\Delta\phi_m = \phi_{Vm} - \phi_E - \phi_I + \phi_{\Delta E} \tag{10}$$

is the measured phase difference including corrections.

As with the magnitude signal, we accommodate the possibility that the phase signal might differ in clockwise ($+\omega$) and counterclockwise ($-\omega$) rotation. Although we have not yet observed this in measurements (see also Appendix C 6), we do not rule it out in our analysis. In analogy to Eq. 4, we decompose the measured phase difference into even (+) and odd (−) components with respect to frequency:

$$\Delta\phi_m(\omega) = \Delta\phi_+(\omega) + \Delta\phi_-(\omega), \tag{11}$$

where

$$\begin{aligned} \Delta\phi_+(\omega) &= (\Delta\phi_m(\omega) + \Delta\phi_m(-\omega))/2 \\ \Delta\phi_-(\omega) &= (\Delta\phi_m(\omega) - \Delta\phi_m(-\omega))/2. \end{aligned} \tag{12}$$

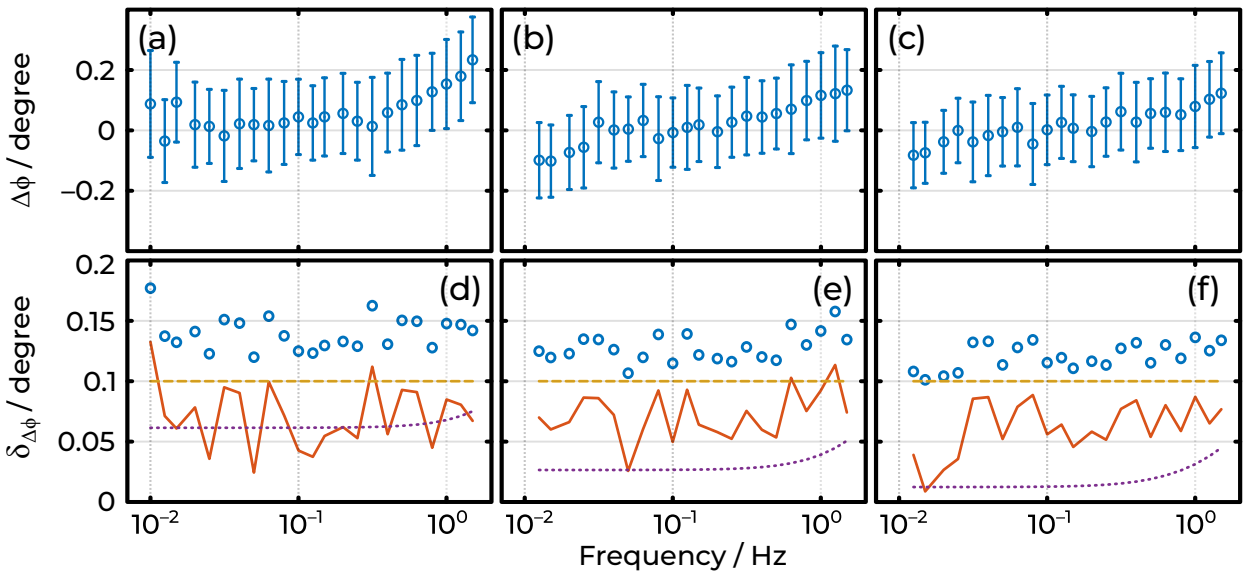

FIG. 4. Phase delay versus frequency with $k = 2$ expanded error bars for accelerometers (a) I, (b) II, and (c) III. (d-f) Corresponding $k = 2$ uncertainty versus frequency. Included are the total uncertainty (blue circles) and constituent uncertainty components (multiplied by k) from Type A (solid red, $\delta_{\Delta\phi,1}$), tilt alignment (yellow dashes, $\delta_{\Delta\phi,3}$), and all others (purple dots).

Because the ideal accelerometer will have $\Delta\phi_-(\omega) = 0$, for the purpose of Eq. 1, we set

$$\Delta\phi = \Delta\phi_+ \tag{13}$$

and ascribe $\Delta\phi_-$ to the uncertainty $\delta_{\Delta\phi,6}$.

Figures 4(a-c) exhibit the mean phase delays measured versus frequency for each accelerometer, along with error bars representing the $k = 2$ expanded uncertainties of the mean. In these cases, observed phase delays lie within $\pm 0.25°$ for all frequencies. Figures 4(d-f) display the calculated uncertainties, including some subcomponents that contribute to the error bars. These uncertainties are the subject of Section III B and Appendix C.

III. UNCERTAINTY

A. Uncertainty in the magnitude of complex sensitivity

We define δ_S, given in $\mathrm{m/s^2}$, as the expanded uncertainty of the determination of S. Then the expanded relative uncertainty, δ_S/S, is calculated as the coverage factor k times

i	Source of magnitude uncertainty	$\delta_{S,i}/S$ in 10^{-6}
1	Statistical variation (Type A)	100
2	Voltage magnitude $\lvert V_{\mathrm{m}}\rvert$ (for $S \approx 0.1$ V/(m s^{-2}))	90
3	Rotation table tilt angle θ (for $\theta \approx \pi/2$)	2
4	Local gravitational acceleration g_l	2
5	Odd-symmetry voltage $\lvert V_{-}(\omega)\rvert$ (non-achiral assumption)	0 to 500
6	Mechanical resonance shift in rotating frame	0 to 100
7	Sensitivity axis misalignment θ_I	10

TABLE I. Components $\delta_{S,i}/S$ contributing to the relative uncertainty δ_S/S, including estimates of their magnitude ($k = 1$). Find detailed descriptions in Appendix B.

the Pythagorean sum of contributing independent relative uncertainty components:

$$\frac{\delta_S}{S} = k\sqrt{\sum_i \left(\frac{\delta_{S,i}}{S}\right)^2} \tag{14}$$

where $\delta_{S,i}$ is the ith uncertainty component of the determination of S. Table I lists the uncertainty components $\delta_{S,i}/S$, and detailed descriptions are found in Appendix B. For conservative simplicity, we assume a normal distribution for all $\delta_{S,i}$. We let δ_S^a denote the uncertainty of S under the achiral assumption (that is, $\delta_{S,5} = 0$). Typical values of the relative uncertainty components appear below. The components $i = \{1, 2, 5, 6, 7\}$ may vary somewhat for each accelerometer, calibration run, and/or frequency. In the accelerometers tested so far, $\delta_S/S \leq 1000 \times 10^{-6} = 0.1$ % (k=2) and $\delta_S^a/S \leq 300 \times 10^{-6} = 0.03$ % (k=2).

Figures 3(d-f) show the calculated δ_S/S for the measurements in (a-c) respectively. Also included for comparison are $k\delta_{S,1}/S$ (Type A), $k\delta_{S,5}/S$ (odd component), and k times the combined others, which in this case are frequency independent. We see that for accelerometers I and III, the odd-symmetry signal contributes a dominant uncertainty for most frequencies, as suggested in Figures 2 (a) and (c). Odd-symmetry aside, the remaining $k = 2$ uncertainties combined are consistently below 0.05 %.

i	Source of phase uncertainty	$\delta_{\Delta\phi,i}$
1	Statistical variation (Type A)	0.04°
2	Angle of intrinsic sensitivity axis ϕ_I	0.03°
3	Accelerometer case alignment to gravity at $\phi = 0$	0.05°
4	Rotation table event trigger angle $\phi_{\Delta E}$	0.01°
5	Voltmeter trigger timing accuracy	0.04°
6	Odd-symmetry phase $\Delta\phi_-(\omega)$	(0 to 0.05)°
7	Mechanical resonance shift in rotating frame	$< 0.01°$

TABLE II. Components $\delta_{\Delta\phi,i}$ contributing to the phase uncertainty $\delta_{\Delta\phi}$, including estimates of their absolute magnitude ($k = 1$). Find detailed descriptions in Appendix C.

B. Uncertainty in the phase of complex sensitivity

The expanded uncertainty of the determination of $\Delta\phi$, $\delta_{\Delta\phi}$ [rad], is calculated as the coverage factor k times the Pythagorean sum of contributing independent uncertainty components:

$$\delta_{\Delta\phi} = k\sqrt{\sum_i \delta^2_{\Delta\phi,i}} \tag{15}$$

where $\delta_{\Delta\phi,i}$ is the i^{th} uncertainty component of the determination of $\Delta\phi$. Table II lists the uncertainty components $\delta_{\Delta\phi,i}$, and detailed descriptions are found in Appendix C. For conservative simplicity, we assume a normal distribution for all $\delta_{\Delta\phi,i}$. Typical values of these components appear below. The components $i = \{1, 2, 6, 7\}$ may vary somewhat for each accelerometer, calibration run, and/or frequency. In the accelerometers tested so far, $\delta_{\Delta\phi} < 0.2°$ (k=2).

Figures 4(d-f) show the calculated $\delta_{\Delta\phi}$ for the measurements in (a-c) respectively. Also included for comparison are $k\delta_{\Delta\phi,1}$ (Type A), $k\delta_{s,3}$ (tilt alignment), and k times the combined others, which in this case have a mild frequency dependence. However, we observe little overall frequency dependence of the uncertainty for all accelerometers, which is consistently below 0.2°.

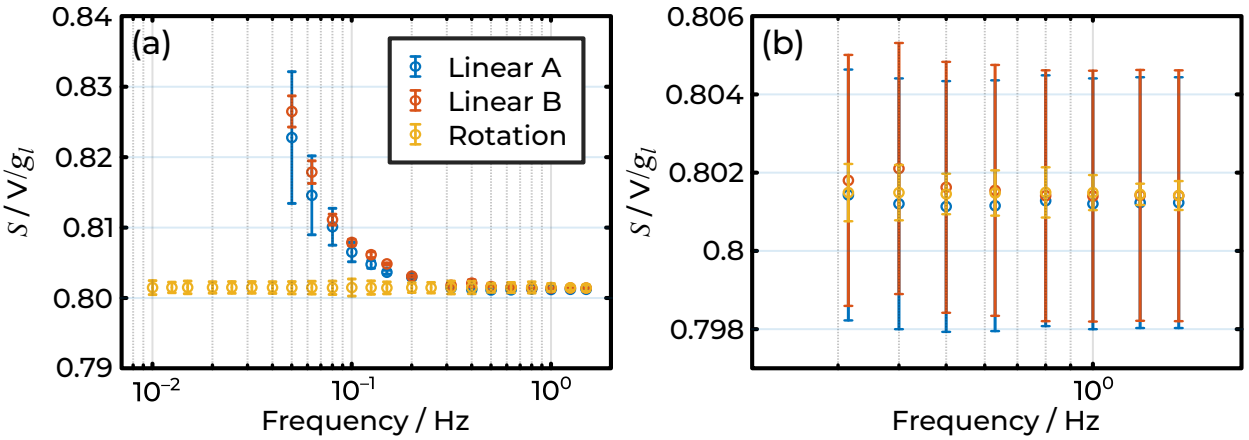

FIG. 5. (a) The sensitivity versus frequency for accelerometer I as measured by two linear shakers and the rotational calibration system. Rotation error bar is δ_S; shaker error bar is standard deviation. (b) Focus on the high frequency data in the range $f = \omega/(2\pi) = (0.315 \text{ to } 1.5)$ Hz. Rotation error bar is δ_S; shaker error bar is $0.004\,S$.

IV. COMPARISON WITH LINEAR SHAKER

To build confidence in the rotary calibration system, we compared it with the established long-stroke-shaker-based systems in our primary accelerometer calibration laboratory. As independent primary acceleration measurement systems, they may serve as mutual checks to establish confidence in each. We measured the sensitivity of accelerometer I using two long-stroke linear shakers in the NIST primary vibration calibration laboratory[6], labeled A and B. Traceability is provided by a laser Doppler vibrometer, and measurements conformed to the ISO standard 16063-11[20].

The sensitivity magnitudes versus frequency extracted from the linear shaker systems, S_A and S_B, appear in Figure 5(a), plotted alongside the rotational data from Figure 3(a), not normalized, S_R. The error bars for S_A and S_B are the standard deviations of repeated measurements, and the error bars for S_R are the values δ_S. We observe that S_R is flat with frequency. In contrast, S_A and S_B deviate from the high-frequency baseline with the characteristic ω^{-2} dependence indicative of the gravity effect, a well-known systematic error in long-stroke shakers[8–10].

Above 0.3 Hz, where the gravity effect is negligible, measurements by both linear and rotational methods show no significant frequency dependence. This higher-frequency regime, including frequencies $f = \omega/(2\pi) = \{0.315, 0.4, 0.5, 0.63, 0.8, 1, 1.25, 1.5\}$ Hz forms the basis

of the comparison. Figure 5(b) focuses on these eight frequencies, with error bars for the shaker data now $0.004\,S_A$ and $0.004\,S_B$, respectively, representing the ($k = 2$) total estimated uncertainty of our long-stroke-shaker-based primary calibrations at those frequencies. We observe that the data all lie within $S_R \pm \delta_S$. This high degree of agreement of independent primary techniques provides confidence in both and even suggests that the shaker estimated uncertainties may be more conservative than necessary.

V. CONCLUSION

We have presented a revived EFDC rotational calibration of accelerometers at NIST. A 2-axis rate table serves as the foundation for a large, consistent, and accurate stimulus. We have performed an uncertainty analysis for measurements of the sensitivity magnitude and phase delay, finding magnitude relative uncertainty below 0.1 % and phase uncertainty below 0.2° ($k = 2$). This technique is limited by the instrumentation to frequencies at and below 1.5 Hz but does not suffer from the systematic errors and low signal magnitude of the linear method below 1 Hz. Thus, it is a valuable complement to existing primary linear calibration techniques, improving magnitude and phase accuracy for compatible accelerometers.

We have demonstrated a magnitude comparison between the rotational and linear approaches over the range (0.315 to 1.5) Hz. This comparison shows excellent agreement to within δ_S and builds confidence in the accuracy of the rotational technique for accelerometer magnitude calibrations.

Finally, the analysis presented here implicitly assumes linearity of the accelerometer primary and cross-axis sensitivities. An upcoming direction of this work is to consider the effect of nonlinearity in an EFDC measurement and to elucidate the role of the EFDC in characterizing accelerometer nonlinearity.

ACKNOWLEDGEMENT

We gratefully acknowledge NIST colleague Akobuije Chijioke for insightful discussions and support.

REFERENCES

[1]W. Wildhack and R. Smith, Proceedings of the Instrument Society of America **9**, 54 (1954).

[2]R. Smith, E. Willis, and J. Hilten, Journal of Research of the National Bureau of Standards, Section C: Engineering and Instrumentation **66C**, 357 (1962).

[3]T. Dimoff and B. F. Payne, Journal of Research of the National Bureau of Standards **67C**, 327 (1963).

[4]J. S. Hilten, "NBS TN 517: Accelerometer Calibration With the Earth's Field Dynamic Calibrator," (1970).

[5]S. Qiao, Metrologia **54**, 09001 (2017).

[6]T. Bruns, Metrologia **58**, 09001 (2021).

[7]E. Sadikoglu, "CCAUV Strategy 2023 - 2033," (2024).

[8]T. Bruns and S. Gazioch, Metrologia **53**, 986 (2016).

[9]G. P. Ripper, C. D. Ferreira, R. S. Dias, and G. B. Micheli, ACTA IMEKO **9**, 365 (2020).

[10]J. H. Strait and R. A. Allen, Metrologia **62**, 015001 (2025).

[11]J. Geist, M. Y. Afridi, C. D. McGray, and M. Gaitan, Journal of Research of the National Institute of Standards and Technology **122**, 32 (2017).

[12]M. Gaitan, I. M. López Bautista, and J. Geist, Metrologia **58**, 035006 (2021), publisher: IOP Publishing.

[13]J. Geist and M. Gaitan, Metrologia **59**, 052101 (2022).

[14]M. Gaitan and J. Geist, Measurement **189**, 110528 (2022).

[15]S. Zhou, C. Cai, Y. Wang, Z. Liu, and M. Yang, in *Tenth International Symposium on Precision Engineering Measurements and Instrumentation*, edited by J. Tan and J. Lin (SPIE, Kunming, China, 2019) p. 93.

[16]C. Jonscher, B. Hofmeister, T. Grießmann, and R. Rolfes, Wind Energy Science **7**, 1053 (2022).

[17]T. Ye, Z. Liu, C. Cai, F. Bao, F. Xu, and X. Lian, Metrology and Measurement Systems , 323 (2024).

[18]Certain commercial equipment, instruments, or materials are identified in this paper in order to specify the experimental procedure adequately. Such identification is not intended to imply recommendation or endorsement of any product or service by NIST, nor is it intended to imply that the materials or equipment identified are necessarily the best available

for the purpose.

[19]T. Shimoda, W. Kokuyama, and H. Nozato, Metrologia **59**, 035010 (2022).

[20]"ISO, International Standard 16063-11, Methods for the calibration of vibration and shock transducers – Part 11: primary vibration calibration by laser interferometry," (1999).

[21]Keysight 3458A User's Guide, Edition 10 (2023).

[22]J. Geist and M. Gaitan, Journal of Research of the National Institute of Standards and Technology **126**, 126038 (2021).

Appendix A: Alignment and Sensitivity

The alignment of an accelerometer is crucial to avoid systematic errors in sensitivity and phase. In addition to the angles θ and ϕ that we control throughout the experiment, we consider the angles θ_I and ϕ_I which represent the misalignment of the accelerometer sensitivity axis in, respectively, the x-z plane and the x-y plane (see Figure 6). Such misalignment may arise from either imperfect mounting or imperfect orientation of the sensitive element with respect to the accelerometer case. As discussed in Sec. II C, ϕ_I is a direct error in the measurement of $\Delta\phi$ and must be corrected. The influence of θ_I is more subtle, including how θ_I differs from an error in θ. Here, we present a simple analysis to disambiguate them and also inform error analysis for any θ.

Consider the rotation matrices about angles θ and ϕ,

$$R_y(\theta) = \begin{bmatrix} \cos\theta & 0 & \sin\theta \\ 0 & 1 & 0 \\ -\sin\theta & 0 & \cos\theta \end{bmatrix} \tag{A1}$$

$$R_z(\phi) = \begin{bmatrix} \cos\phi & -\sin\phi & 0 \\ \sin\phi & \cos\phi & 0 \\ 0 & 0 & 1 \end{bmatrix} \tag{A2}$$

which act on the sensitivity three-vector both during the experiment and also due to misalignment. For $\theta = \phi = 0$, the case-normal vector (i.e. the nominal sensitivity vector assuming no misalignment) is $\vec{S} = (1, 0, 0)$. Then, assuming $\phi_I = 0$ for this analysis of the sensitivity magnitude, the actual vector of sensitivity is $\vec{S}_I(\theta_I) = R_y(\theta_I)\vec{S} = (\cos\theta_I, 0, -\sin\theta_I)$.

During the experiment setup and operation, the accelerometer rotates by angles θ and ϕ

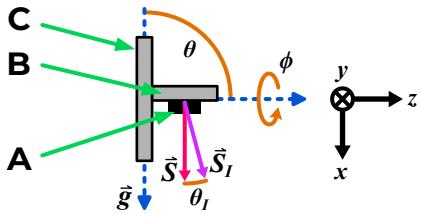

FIG. 6. Cross-section diagram (not to scale) of the accelerometer (A), 90° bracket (B), and rotation table (C), shown oriented with $\theta = \pi/2$. For $\theta = \pi/2$ and $\phi = 0$, the case-normal vector $\vec{S}$ is nominally parallel to the gravity vector $\vec{g}$ and perpendicular to the rotation axis z. The sensitivity vector $\vec{S}_I$ may deviate from $\vec{S}$ by, for instance, a rotation in the x-z plane of θ_I.

such that

$$\vec{S}_I(\theta_I, \phi, \theta) = R_y(\theta) R_z(\phi) \vec{S}_I(\theta_I). \tag{A3}$$

The stimulus applied to the accelerometer sensitive element will be $\vec{g} \cdot \vec{S}_I(\theta_I, \phi, \theta)$, where $\vec{g} = g_l(0, 0, -1)$ is the gravity vector. Setting $\phi = \omega t$ and switching to complex phasor representation analogous to Eq. 2, we find the corrected stimulus

$$a_c(t) = g_l(\cos(\theta_I)\sin(\theta)e^{i\omega t + \phi} + \cos(\theta)\sin(\theta_I)). \tag{A4}$$

We see that θ_I introduces a static signal and also modifies the oscillating component. Following sine-wave fitting or Fourier filtering at frequency ω as described in Sec. II B, we find

$$A_c = g_l \cos(\theta_I)\sin(\theta)e^{i\phi}, \tag{A5}$$

which differs from the perfectly aligned stimulus a found in Eq. 2 by a factor of $\cos(\theta_I)$.

Equation A5 reveals the difference between how θ and θ_I contribute to measurement errors, which originates from the fact that θ affects the rotation axis and θ_I does not. Let $\delta\theta$ be the uncertainty in θ. In the context of the measurements presented here, $\theta = \pi/2 + \delta\theta$, and we assume $\{\theta_I, \delta\theta\} \ll \pi/2$. So $a_c \propto \cos\theta_I \cos\delta\theta \approx (1 - \theta_I^2/2)(1 - \delta\theta^2/2)$ to lowest order, and θ_I and $\delta\theta$ influence a in the same way: as second order corrections. However, for $\theta \to 0$, $a_c \propto \cos\theta_I \sin\delta\theta \approx (1 - \theta_I^2/2)\delta\theta$, resulting in a comparatively large uncertainty.

Appendix B: Magnitude Uncertainty Components

1. $\delta_{S,1}$ – Statistical variation (Type A)

Let $\sigma_+(\omega)$ and $\sigma_-(\omega)$ be the standard deviations of accelerometer sensitivity magnitude extracted for clockwise and counterclockwise rotations at frequency ω. We use $\delta_{S,1} = \sqrt{\sigma_+(\omega)^2 + \sigma_-(\omega)^2}$. The value of $\delta_{S,1}$ depends on measurement parameters and the accelerometer itself, and we calculate it for each measurement. In the accelerometers tested so far, we find $\delta_{S,1}/S \leq 100 \times 10^{-6}$. Long-term drift on the time scale of a month or more has been negligible.

2. $\delta_{S,2}$ – Voltage magnitude $|V_{\mathbf{m}}|$

We count five independent contributions to the voltage magnitude measurement uncertainty:

$$\delta_{S,2} = \sqrt{\delta V_{\mathrm{DVM}}^2 + \delta V_s^2 + \delta V_p^2 + \delta V_\omega^2 + \delta V_a^2}. \tag{B1}$$

Descriptions of these sub-components appear below. We find $\delta_{S,2}/S \leq 90 \times 10^{-6}$ for all frequencies for accelerometers with sensitivity $S \approx 0.1$ V/(m s^{-2}).

a. Digitizing voltmeter calibration - δV_{DVM}

We use auto-calibrated Keysight 3458A voltmeters in DC sampling mode. With 100 μs aperture time, for accelerometers with sensitivity ≥ 1 mV/(m s^{-2}), and for excitation magnitude ≈ 9.8 m/s^2, the relative magnitude error is specified within (15×10^{-6})[21]. Our own intercomparisons of 3458A instruments in our lab calibrated at different times using these data sampling parameters show agreement to better than 40×10^{-6}, expressed as a relative difference. For $\delta V_{\mathrm{DVM}}/S$, we conservatively allow 50×10^{-6} relative magnitude uncertainty.

b. Finite sampling time - δV_s

This error arises due to convolution of the measured sine wave with finite sampling (aperture) time. With 100 μs aperture time and a maximum rotation frequency < 3 Hz, $\delta V_s/S$ is insignificant at $< 1 \times 10^{-6}$.

c. Parasitic signal coupling - δV_p

We acknowledge the possibility of parasitic signals oscillating at ω coupling to and generated within wires. Such signals would be a systematic error in the magnitude measurement. We estimated the scale of this error by replacing an accelerometer with a passive dummy circuit consisting of a resistor and capacitor in parallel to approximate the accelerometer electrical impedance. The cable on the rotating table was secured in a manner consistent with accelerometer measurements. The data, collected and analyzed as usual, revealed parasitic signal magnitudes consistently under 40 μV, corresponding to a relative error of $40\ (\mu\mathrm{V}/A)/S = 50 \times 10^{-6}$ for $S = 0.8\ \mathrm{V}/g_l$.

d. Rotation frequency - δV_ω

Sine wave magnitude extraction by Fourier analysis is most accurate for sampling of an integer number of waveforms[19]. Since the rotation table controller clock is independent of the sampling clock, the agreement of these clocks is an implicit assumption. We compared data extraction by Fourier magnitude to that by sine fitting, which agreed to within a 1×10^{-6} relative difference for all frequencies, setting the limit of uncertainty from this effect.

e. Stimulus anharmonicity - δV_a

The data processing implicitly assumes time harmonicity of acceleration stimulus a. To satisfy this requirement, the rotation table must have a constant angular velocity, given the relative constancy of g_l with time to the $< 10^{-6}$ level. We evaluate this assumption by analysis of the angular velocity error versus time using a velocity error signal provided by the rotation table. The measured angular velocity noise adds an error on the voltage magnitudes which we estimate with Fourier analysis. We find that the relative uncertainty contribution $\delta V_a/S$ is frequency dependent, ranging from $\approx 50 \times 10^{-6}$ at 10 mHz down to $< 5 \times 10^{-6}$ at 1.5 Hz.

3. $\delta_{S,3}$ – Rotation table tilt angle θ

As described in Appendix A, misalignment of the rotation axis by an angle $\delta\theta$ when $\theta \approx \pi/2$ leads to a change in V_m by a factor of $\cos\delta\theta$. The rate table we use has a specified angular position accuracy of ± 30 arcsec $\approx 0.01°$. In addition, we have observed a tilting wobble in the rotation plate using a bubble level with $0.01°$ precision as the plate revolves in static steps. The maximum static tilt deviation observed is approximately $0.04°$; however, acknowledging that dynamic wobble may exceed static wobble, we estimate a maximum deviation value of $0.1°$ up to 1.5 Hz, pending refinement following further measurements. Although a distribution of deviations up to $0.1°$ would affect V_m to a lesser extent than a static error of the same value, we conservatively assign $\delta\theta = 0.1°$, and so $\delta_{S,3}/S = |1 - \cos(\delta\theta)| \approx 2 \times 10^{-6}$.

4. $\delta_{S,4}$ – Local gravitational acceleration g_l

We trace the local value of gravitational acceleration to the National Geodetic Survey published by the National Oceanographic and Atmospheric Administration as earlier interpreted[22] for the vicinity of the rotation table in the NIST Sound Building to be $g_l = 9.80101 \pm 0.000015$ m/s^2 ($k = 1$). We therefore use $\delta_{S,4}/S = 2 \times 10^{-6}$.

5. $\delta_{S,5}$ – Odd-symmetry voltage $|V_-(\omega)|$

Accelerometer sensitivity that has odd symmetry with respect to the rotation direction (see Section II B) is evidence of measurement chirality either intrinsic or extrinsic to the accelerometer. If we have reason to believe the chirality is extrinsic (i.e. the accelerometer construction is achiral, but perhaps it is sensitive to the magnetic fields of the rotation table), then this effect would not carry over to measurements of linear acceleration in the field. In this case, we may regard the calculation of $|V_+(\omega)|$ as an effective correction and $\delta_{S,5} = 0$. Generally, the achiral assumption is not recommended due to potential accelerometer manufacturing or design defects. More conservatively, we use $\delta_{S,5} = |V_-(\omega)|/|a|$ and $\delta_{S,5}/S = |V_-(\omega)|/|V_+(\omega)|$, which for accelerometers measured so far ranges from (0 to 500)$\times 10^{-6}$ (see examples in Figure 3).

6. $\delta_{S,6}$ – Mechanical resonance shift in rotating frame

The mechanical resonance of an accelerometer shifts and distorts in a rotating frame compared to a linear frame due to the centrifugal force. Following Wildhack and Smith (1954)[1] and modeling the accelerometer as a spring-mass-damper resonator, the equation of motion of the mass is

$$M\ddot{x} + s\dot{x} + Kx = Mg_l \cos(\omega t) + \alpha(M\omega^2 r_0 + M\omega^2 x) \tag{B2}$$

Where M is the mass, s is the damping constant, K is the stiffness, r_0 is the constant radial displacement of the mass, x is the time-varying radial deviation of the oscillating mass, and $\alpha = \{0, 1\}$ for a {linear, rotating} frame. The resulting ratio between the dynamic and static response (the "instrument response ratio") is[1,4]

$$R_\alpha = \left[(1 - (1+\alpha)\epsilon^2)^2 + 4p^2\epsilon^2\right]^{-1/2} \tag{B3}$$

where $p = s/(2M\omega_n)$ is the damping ratio, $\epsilon = \omega/\omega_n$, and $\omega_n = \sqrt{K/M}$. The difference between R_0 and R_1 is an error in measured sensitivity for accelerometers to be used in a linear frame, and it depends on the operating frequency via ϵ. We treat this difference as the uncertainty $\delta_{S,6}/S = R_1/R_0 - 1$. For $\epsilon \to 0$, $\delta_{S,6}/S \approx \epsilon^2$. Our worst-case frequency is $f = \omega/2\pi = 1.5$ Hz, and with a relatively low resonance frequency of 150 Hz, $\delta_{S,6}/S = 100 \times 10^{-6}$. For accelerometers measured so far with $\omega_n > 1$ kHz, $\delta_{S,6}/S$ is negligible at $< 10 \times 10^{-6}$.

7. $\delta_{S,7}$ – Sensitivity axis misalignment θ_I

As described in Appendix A, misalignment of the accelerometer sensitivity axis by an angle θ_I in the x'-z' plane leads to a change in V_m by a factor of $\cos\theta_I$. We distinguish two sources of this misalignment: (i) imperfect mounting of the accelerometer case ("extrinsic") and (ii) imperfect alignment of the sensitive element within the case ("intrinsic"). Intrinsic misalignment will affect the operation of the accelerometer equally whether in a linear-frame or rotational-frame measurement. Thus, we do not consider intrinsic misalignment an error for the purposes of this calibration.

To characterize the extrinsic misalignment, we use a bubble level accurate to $\approx 0.25°$ placed on the accelerometer at $\theta = \pi/2$ and $\phi = \pi$ to verify the alignment of the case

with gravity in this configuration. We use the upper bound $\theta_I = 0.25°$, and therefore $\delta_{S,7}/S = |1 - \cos(\theta_I)| \approx 10 \times 10^{-6}$.

Appendix C: Phase Uncertainty Components

1. $\delta_{\Delta\phi,1}$ – Statistical variation (Type A)

We use the standard error of the mean $\Delta\phi$, SE $= \sigma_{\Delta\phi}/\sqrt{N}$, where $\sigma_{\Delta\phi}$ is the standard deviation of phase difference measurements and N is the waveform sample size (typically $N = 10$). In accelerometers tested to date, we find $\delta_{\Delta\phi,1} \leq 0.04°$. Long-term drift on the time scale of a month or more has thus far been negligible.

2. $\delta_{\Delta\phi,2}$ – Angle of intrinsic sensitivity axis ϕ_I

We establish ϕ_I with a quasi-static step-rotation measurement following the frequency sweep. Typical measurement parameters include 5° steps and a 10 s settling time between steps. By fitting the resulting sinusoid voltage versus angle, we extract ϕ_I with a fitting uncertainty. In accelerometers tested so far, this uncertainty is $\delta_{\Delta\phi,2} \approx 0.03°$.

3. $\delta_{\Delta\phi,3}$ – Accelerometer case alignment to gravity

We align the accelerometer mount such that the mounting surface is normal to gravity at $\theta = \pi/2$ and $\phi = 0$ (as defined by the rotation table internal position encoder). Any rotational misalignment in the x-y plane is a direct error for $\Delta\phi$. We confirm this alignment with a bubble level with 0.02° standard uncertainty. Considering the manufacturing tolerances of the bracket, we allow for a total rotational angle uncertainty of $\delta_{\Delta\phi,3} = 0.05°$.

4. $\delta_{\Delta\phi,4}$ – Event trigger angle

We determine the event trigger angle $\phi_{\Delta E}$ with a recursive search of static angular steps while monitoring the angle at which the event signal goes from low to high. Given the repeatability of this process and accuracy of the position encoder, we take this uncertainty to be $\delta_{\Delta\phi,4} = 0.01°$.

5. $\delta_{\Delta\phi,5}$ – Voltmeter trigger timing accuracy

Notwithstanding the trigger timing accuracy specifications of the voltmeter, timing errors may arise between nominally synchronized voltmeters due to, for example, cables and software. We have measured such errors using a synthetic waveform simultaneously applied to the voltmeters which measure ϕ_V and ϕ_E during the calibration. We extract the relative phase delay $\Delta\phi_V$ between voltmeters by Fourier analysis and plot it versus time. Then we compute a fixed time delay, $\Delta t_V \pm \delta_{\Delta t}$, by ordinary linear least-squares fitting, where the uncertainty is the $k = 1$ confidence based on the fit alone. The extracted value applies to future recalculations of the phase correction at any frequency: $\phi_V = \omega\Delta t$. The frequency-dependent uncertainty $\delta_{\Delta\phi,5} = \omega\delta_{\Delta t} \approx 0.036°$ for the worst-case frequency $f = \omega/2\pi = 2.5$ Hz.

6. $\delta_{\Delta\phi,6}$ – Odd-symmetry phase $\Delta\phi_-(\omega)$

The phase difference with odd symmetry versus frequency, $\Delta\phi_-(\omega)$ (see Section II C), is a systematic error because an ideal accelerometer will have $\Delta\phi_-(\omega) = 0$. In cases where $\Delta\phi_-(\omega)$ is statistically different from zero, as determined by a one-sample t-test with 0.05 significance, we set $\delta_{\Delta\phi,6} = |\Delta\phi_-(\omega)|$. For accelerometers measured so far, we have exclusively measured values of $\Delta\phi_-(\omega)$ statistically indistinguishable from zero. In these cases, we set $\delta_{\Delta\phi,6} = 0$ to avoid double-counting noise.

7. $\delta_{\Delta\phi,7}$ – Mechanical resonance shift in rotating frame

Mechanical resonance shift due to centrifugal force affects the phase delay of an accelerometer response in a rotating frame compared to a linear frame. The phase response of the accelerometer modeled as in Section B 6 is[1]

$$\Phi_\alpha = \tan^{-1}\left[\frac{2p\epsilon}{(1-(1+\alpha)\epsilon^2)}\right], \tag{C1}$$

using symbol definitions from Section B 6. We assign the phase delay between linear and rotational frames to the uncertainty $\delta_{\Delta\phi,7} = |\Phi_1 - \Phi_0|$. It is negligible at $< 0.01°$ for frequency ratio $\epsilon \leq 0.01$ (e.g. for resonance frequency ≥ 150 Hz for the worst-case operating frequency

1.5 Hz). For accelerometers operated closer to resonance, this delay may be significant depending on the accelerometer mechanical damping.